

## Radar analysis of a tornado over hilly terrain on 23 July 1996

Ronald Hannesen<sup>1</sup>, Nikolai Dotzek<sup>2</sup>, and Jan Handwerker<sup>3</sup>

<sup>1</sup> Gematronik GmbH,

Raiffeisenstr. 10, D–41470 Neuss, Germany

<sup>2</sup> DLR–Institut für Physik der Atmosphäre,

Oberpfaffenhofen, D–82234 Wessling, Germany

<sup>3</sup> FZK–Institut für Meteorologie und Klimaforschung,

Postfach 3640, D–76021 Karlsruhe, Germany

### Proc. 1st European Conference on Radar Meteorology

*Received 15 Jun 2000, in final form 15 Jul 2000*

#### Corresponding author's address:

Dr. N. Dotzek

DLR–Institut für Physik der Atmosphäre,

Oberpfaffenhofen, D–82234 Wessling, Germany.

E-mail: Nikolai.Dotzek@dlr.de,

Tel: +49–8153–28–1845, Fax: +49–8153–28–1841.

# Radar analysis of a tornado over hilly terrain on 23 July 1996

Ronald Hannesen<sup>1</sup>, Nikolai Dotzek<sup>2</sup>, and Jan Handwerker<sup>3</sup>

<sup>1</sup> Gematronik GmbH,

Raiffeisenstr. 10, D–41470 Neuss, Germany

<sup>2</sup> DLR–Institut für Physik der Atmosphäre,

Oberpfaffenhofen, D–82234 Wessling, Germany

<sup>3</sup> FZK–Institut für Meteorologie und Klimaforschung,

Postfach 3640, D–76021 Karlsruhe, Germany

*Received 15 Jun 2000, in final form 15 Jul 2000*

## Abstract

A Doppler radar case study of an F1–2 tornado in the Upper Rhine valley in Germany is presented. The Ziegelhausen tornado touched down on the hilly terrain near Heidelberg in the evening of 23 July 1996. A mini-supercell was the parent storm of the short-lived funnel. During its intensification the Cb-cell behaved like an ordinary right-moving supercell, but along with transition to its tornadic phase a hook echo developed at the storm's right rear flank, indicative of *anticyclonic* rotation. In addition a mesocyclonic in-cloud vortex signature was found higher up and proved to be more persistent than the small anticyclonic circulation at the hook echo tip. So both, parent storm and tornado vortex were most likely cyclonic, with the damage swath to the left of the mesocyclone's ground track. The false anticyclonic hook echo appeared to be caused by small-scale orographic forcing. Terrain structure near the tornado site may have induced a low-level anticyclonic lee-vortex in the wake of an isolated mountain. Vertical vorticity advection and orogenic horizontal deformation of the airflow could then serve to consistently explain both the false hook and its sense of rotation. Climatologically, the Ziegelhausen tornado was representa-

tive for most German tornado outbreaks. Neither was the parent thunderstorm nowcast as potentially tornadic nor was any warning issued to the public.

## 1 Introduction

The Upper Rhine valley in SW Germany (cf. Fig. 1 showing this area and places mentioned in our paper) is a region with frequent thunderstorm (Cb) development (e. g. Finke & Hauf, 1996; Hagen et al., 1999). Since the early 1990s the operational C–band Doppler radar at Forschungszentrum Karlsruhe (about 10 km N of the city, + in Fig. 1) serves as an efficient means to study deep convection over this highly structured terrain and its implications for areal precipitation (Gysi, 1998). For basic research of convection–terrain interactions the radar has also been applied recently (Hannesen, 1998) along with mesoscale modelling studies (Dotzek, 1999). This work lead to the conclusion that on days with strong thunderstorm activity there is also considerable probability of severe weather (Dotzek et al., 1998; Dotzek, 2000).

For instance, since the buildup of the radar in 1992 at least four tornadic storms have occurred within the standard 120 km radar range: 21 July 1992 near Rastatt, 9 September 1995 at Oberkirch–Nußbach (**N** in Fig. 1), 23 July 1996 at Ziegelhausen near Heidelberg (**Z** and **H** in Fig. 1) and 1 May 1998 at Pfungstadt–Hahn (in 1992 the radar was not yet operative, in 1998 it was off due to technical reasons). As Hannesen et al. (1998) had studied the 1995 Nußbach tornado, the 1996 Ziegelhausen tornado will be the subject of our present paper. The storm was at close range (roughly 50 km) to Karlsruhe C–band Doppler radar, even closer than during the 1995 outbreak (about 70 km). After evaluation of the 1996 data we compare these two events both having originated from mini–supercell storms (cf. Kennedy et al., 1993).

The paper is organized as follows: in Sec. 2 we describe the synoptic setting on 23 July 1996. Sec. 3 presents the radar data analysis of the tornadic storm. Our results are discussed and compared to the 9 September 1995 Nußbach tornado in Sec. 4. Conclusions are drawn in Sec. 5.

## 2 Synoptic setting

On 23 July 1996 strong convective cells developed over the Netherlands around midday and over Germany in the afternoon and evening, spawning one weak tornado in each country. Fig. 2

illustrates the synoptic situation at 1200 UTC.

Central European weather was dominated by a depression located at the Netherlands' North Sea coast. The cold front of this system stretched out from N to S and propagated eastward. Approximately 350 km ahead of this cold front and nearly parallel to it, a strong convergence line extended from northern Germany towards the Alps. This convergence line lead to widespread deep convection being significantly stronger than that of the actual cold front. As reported by Terpstra (2000), about at that time a weak tornado occurred in the Netherlands within an environment of high convectively available potential energy (CAPE) of  $1800 \text{ J kg}^{-1}$  and substantial helicity of  $160 \text{ J kg}^{-1}$ . As pointed out by Brooks et al. (1994) this would imply an energy–helicity index of 1.8 and therefore even the chance of strong tornadoes. However, in Switzerland and Germany the CAPE values were not as high, decreasing southward and eastward to about  $700 \text{ J kg}^{-1}$  in Payerne (Huntrieser et al., 1998) and Munich, respectively. Here the tropopause was at about 10 km above mean sea level (ASL). Nevertheless, thunderstorms over Germany were still intense and chosen to be studied within the LINOX experimental campaign (Huntrieser et al., 1998; Höller et al., 1999) in southern Germany, providing by chance a large database for our present case study.

The cold front progressed eastward with a mean translational speed of more than  $40 \text{ km h}^{-1}$  (Terpstra, 2000), so the frontal convection reached south–western Germany at about 1700 UTC. At this time a line–shaped thunderstorm complex had formed over the Palatinian Mountains (600 m ASL) and entered the very flat and low–level (about 100 m ASL, cf. Fig. 1) Upper Rhine valley. About one hour later the tornado touched down.

### 3 Analysis of the radar data

Karlsruhe C–band Doppler radar raw data ( $500 \text{ m} \times 1^\circ$  bin size) were processed for our analysis to a high horizontal cartesian pixel resolution of  $250 \times 250 \text{ m}^2$ . This was possible due to the storm's short distance of 40 to 60 km from the radar site. Consecutive locations of the intensifying Cb–cell during transition to its tornadic phase and later decay are given in Fig. 3 (bullets). The equally–spaced time steps one to ten denote 1658, 1708, . . . , 1828 UTC. The tornado site (**T**) between the 1758 and 1808 UTC radar scans is indicated by an arrow. In general the parent storm moved from W to E with a mean speed of  $(u, v) = (18.3, 1.7) \text{ m s}^{-1}$  corresponding to about  $66 \text{ km h}^{-1}$ . Note the slight turn towards the north after the storm had

entered the hilly terrain of the Odenwald NE of the radar: in principle the cell travelled straight along the Neckar river valley. Tab. 1 adds further quantitative information on storm evolution between 1648 and 1918 UTC: both radar echo top  $H_{25}$  dBZ and reflectivity factor Z peak during the tornado outbreak.

Over the Rhine valley basin the line-shaped storm evolved first into a bow-shaped cell, then into a compact structure with two and later only one distinct reflectivity core (first at 1758 UTC). At this time the storm entered the Neckar valley at Heidelberg and became tornadic. The funnel touched down shortly after 1800 UTC, uprooting or snapping even mature beech and spruce trees (implying T4/F1–2 intensity) and injuring several people driving in cars. The funnel's miso-vortex developed to the left side of the cell's ground track and then crossed over a N–S oriented lateral valley of the Neckar river, sparing the village of Ziegelhausen, but causing a roughly 5 km long forest damage swath within about 5 min (Dittmar, 1998). During and after this stage the storm formed very heavy precipitation and moved E, only slowly decaying and becoming multicellular again.

As a site investigation revealed, the radar was not able to detect the funnel itself due to the 600 m high Königstuhl mountain range directly adjacent southward to the Neckar river. So only for elevations above  $2^\circ$  (about 2 km above radar at 50 km range) radar data evaluation is meaningful.

Note that plan position indicator (PPI) scans at several elevations revealed that the Cb's core was tilted forward roughly in the direction of mean storm motion. Fig. 4 focuses on lower elevation angles and shows a composite of the  $3^\circ$  reflectivity and Doppler velocity PPIs of 1808 UTC (a) and 1828 UTC (b) over an enlarged area of the terrain in Fig. 1. These two times correspond to the points 8 and 10 in Fig. 3. Range rings are given every 20 km and the tornado position is indicated by the arrow. The storm's area is contoured by the 20 dBZ (hatched) and 43 dBZ (cross-hatched) reflectivity thresholds. Vortex signatures derived from the measured Doppler velocity are given by the small (anticyclonic) and the larger circular arrows (cyclonic).

In Fig. 4 a, about the time of tornado touchdown, the radar echo is dominated by a compact core of high reflectivity factor just E of the tornado position. In addition strong radar beam attenuation is noticeable: both storm contours are V-shaped with a wedge-shaped reflectivity gap at larger distance from the radar. As shown in Tab. 1 the reflectivity factor Z peaked between 55 and 60 dBZ in this storm. Such a high intensity indicates heavy rain or hail in the thundercloud, even though no hail spike was visible in PPI displays.

The Doppler data show a mesocyclonic vortex signature (MVS) on the east, forward flank of the storm core. Significant mesocyclonic rotation is clearly detectable in the radar data from 1728 UTC on and intensifying between 1748 and 1808 UTC over the hilly terrain simultaneous to cloud growth to its highest echo top. At this time the MVS diameter was about 8 km and its vertical dimension was 3 km, extending from roughly 2 to 5 km above ground level. The mesocyclone had a velocity difference of 23 to 27  $\text{m s}^{-1}$  leading to a horizontal shear of  $0.003 \text{ s}^{-1}$ , slightly less than for the Nußbach tornado (Hannesen et al., 1998), but with a larger mesocyclone.

At the southern edge of the storm a small but distinct bow or hook-shaped radar echo extends outward from the Cb-core. As the reflectivity within this hook-like echo exceeds 43 dBZ it is not likely that it was caused by the propagation of a gust front caused by precipitation-induced thunderstorm outflow. But if this structure were a real hook echo, then its curvature would imply the presence of an anticyclonic tornado. This rare type of tornado requires an environmental wind vector backing with height instead of veering as in the typical right-moving supercell situation.

The Doppler velocity data in the area of this hook echo are sparse due to technical limitations, but nevertheless a vortex signature (smaller and weaker than the mesocyclone) can be diagnosed. Its rotational sense is indeed anticyclonic and consistent with the southern end of the anticyclonic hook echo. So this result raises the question if it is evidence for an anticyclonic tornado vortex signature (TVS) or if this hook echo was caused by other dynamical effects and presents a *false hook* (Houze et al., 1993). The tornado damage swath is closer to the track of the larger mesocyclone, but as the  $3^\circ$  radar beam is at about 2.5 km above radar, i. e. roughly 2 km over the largest terrain heights it cannot completely ruled out from the first that the funnel extended from the anticyclonic hook echo northward to the observed damage path.

To clarify the situation the  $3^\circ$  PPI-composite at 1828 UTC (Fig. 4 b, after the tornado had already lost ground contact or had dissipated completely for about 10 min) still shows the large cell core and the anticyclonic hook echo, now at 3.5 km above radar due to the increased radial distance. The storm has grown in size, retaining maximum reflectivities between 55 and 60 dBZ, but with a descending echo top (cf. Tab. 1). Although not clearly apparent in this picture, radar beam attenuation at higher elevations is even stronger than for the time of tornado touchdown. Doppler velocity information still indicates the presence of the cyclonic MVS, but no more anticyclonic rotation can be inferred near the southern end of the hook echo. It must be stated,

however, that the Doppler data for this scan are again quite sparse, especially at the lower elevation angles. But while the cyclonic MVS is found in several elevations, no such evidence for anticyclonic rotation near the hook echo tip was found at 1828 UTC. However, the hook structure remains visible at several elevation angles, not only at  $3^\circ$ . Yet for a true anticyclonic hook a wind backing with height would require a southerly flow component atop the low-level south–westerly flow in the Neckar valley. But this is not supported by our observations.

Concerning the tornado’s sense of rotation, we argue that this small supercell was of the usual cyclonic (right-moving) type and the hook echo is really a false hook. Several observations support this judgement. First, the larger cyclonic MVS is much more persistent than its smaller anticyclonic counterpart. Second, after entering the Upper Rhine valley from the Palatian Mountains the Cb-cell developed its in-cloud rotation and showed a storm motion to the right of the environmental mid-level flow. Third, backing winds with height are not plausible for this synoptic setting, and fourth, the ground track of the cyclonic MVS matched the tornado damage swath better than the anticyclonic hook.

## 4 Discussion

The source of the unusual hook-shaped reflectivity structure which appears to be too strong and too high up to stem e. g. from an arc-shaped cloud line of a thunderstorm outflow is not obvious from the radar data alone. Yet taking into account the small-scale terrain shape in the region where the tornado formed and the Cb reached its highest echo top of 12.5 km ASL yields a plausible concept for explanation.

Fig. 5 shows a sketch of any relevant orographic structures within a radius of about 10 km around the tornado path (bold dashed line) together with the radar-observed mesocyclone’s ground track (dashed open arrow) and a probable low-level flow field (bold solid arrows). The best candidate for orogenic anticyclonic vorticity generation is the isolated and almost 600 m ASL high Königstuhl mountain. With the mountain ranges N of the Neckar river the Königstuhl likely served as a nozzle for the westerly airflow of the approaching thunderstorm, inducing flow convergence, lifting, updraft intensification and cloud growth (cf. Tab. 1) as the Cb-cell entered the Neckar valley and became tornadic.

Due to the orographically enhanced horizontal mass flux and the sudden broadening of the Neckar valley E of the Königstuhl (the “nozzle outlet”) it is not unlikely that in the wake of

this mountain a transient lee–vortex developed during the passage of the tornadic Cb–cell. Apparently, such a lee–vortex must have had an anticyclonic sense of rotation. Comparing this conceptual low–level flow configuration with the hook echo position of Fig. 4 and the small anticyclonic MVS therein, we find a good agreement between the two. We might argue that this anticyclonic vorticity was vertically advected both by the storm’s updraft and orographic lifting over the flatter hills E of Königstuhl mountain. Thereby we could explain both the weaker anticyclonic MVS in the 3° PPI and the false hook echo. The former was then due to vorticity advection, the latter due to the horizontally diverging, but rising airflow in the Neckar valley which might have stretched the southern edge of the storm’s precipitation region towards the SW. Also, it is reasonable that the weak anticyclonic rotation decayed soon after the storm moved further E from the lee–vortex position, while the hook–like cloud structure developed in an unstably stratified environment and could still be observed at 1828 UTC in Fig. 4 b. This explanation is definitely conceptual, but well–supported by the presently available observations. The underlying dynamics may be evaluated in the future using LINOX data and fine–scale model simulations. The archives of the LINOX campaign (Huntrieser et al., 1998; Höller et al., 1999) contain much additional information on the thunderstorms of 23 July 1996. This includes 2D–lightning observations, radiosonde and polarimetric Doppler radar data from POLDIRAD in Oberpfaffenhofen which detected the tornadic storm at quite large range but tracked its easterly progression after the Cb had left Karlsruhe radar range.

Both the 1995 and 1996 tornadic mini–supercellular storms analyzed from Karlsruhe radar data show many similar aspects, except for one: the Nußbach tornado (Hannesen et al., 1998) *dissipated* after it had entered the hilly terrain of the northern Black Forest. On the contrary, the tornado near Heidelberg *formed* after the Cb–cell had moved from the flat Rhine valley to the hilly Odenwald terrain. It should be noted that both tornadoes touched down in regions where valleys from the surrounding mountains open into the large Upper Rhine valley — the broader Neckar valley in the 1996 case and the narrow Rench valley in the 1995 case. However, on 9 September 1995 several supercells formed amidst the Upper Rhine valley, one of which became tornadic soon enough before the first (and gently sloping) hill ranges were reached. Here the mechanisms for tornado formation were linked to the wind shear within the Rhine valley, so the first hills disturbed the low–level tornadic wind field, thereby dissipating the funnel. On 23 July 1996 the situation was different: the transition from the Rhine valley base to the hills near Heidelberg is quite abrupt and the thunderstorm–related inflow from the Upper

Rhine valley into the steep and nozzle-like Neckar valley must have been the main trigger for tornado genesis in this case.

The tornado studied here was not exceptional: the Upper Rhine valley is a quite tornado-prone region in Germany, leading to a tornado alley from W to E (Hannesen et al., 1998; Dotzek, 2000) as well as to a preference for non-severe convection in that area (Gysi, 1998; Hannesen, 1998). From the standpoint of a German tornado climatology following the work of Wegener (1917), an evaluation of the TorDACH data showed that July is the most likely month for tornado outbreaks, and 4 to 7 tornadoes occur on average each year Dotzek (2000). So case studies like the present one also contribute to our knowledge of the severe storms climatology in Germany and follow the concepts originally developed by Johannes Letzmann during the first half of the 20th century (cf. Peterson, 1992; Dotzek et al., 2000).

In general this Doppler radar study as well as the earlier one by the authors (Hannesen et al., 1998) substantiated the usefulness and the difficulties in detecting and analyzing severe thunderstorms in Germany by radar. Both tornadic thunderstorms leading to the 23 July 1996 and the 9 September 1995 tornadoes were of the mini-supercell type (Kennedy et al., 1993; Suzuki et al., 2000). This storm type shows characteristics of classical supercells but is about a factor of two smaller in size. Nowcasting this storm type with C-band Doppler radars as the one in Karlsruhe (or those operated by the German weather service DWD within their national radar network) is not a simple task: radar structures like a hook echo, the mesocyclone or even tornado vortex signatures are quite small in these storms. Besides, mini-supercells can be rather short-lived and the transition to their tornadic phase may be overlooked between two consecutive routine radar volume scans.

However, both our analyses also proposed that Doppler radar measurements are currently the most promising means to increase our knowledge on tornadoes and other severe thunderstorm phenomena in Central Europe. If tornadic damage is reported, analyzing archived radar data will be helpful to understand the tornado's specific genesis mechanisms. Case studies like ours and, e. g., Schmid et al. (1997) may serve as test bases for the application of severe storm detection algorithms which should eventually lead to an operational automatic monitoring and warning system for nowcasting severe storms in Europe.

## 5 Conclusions

From our case study of the 23 July 1996 tornado outbreak near Heidelberg we conclude

1. the storm was of a mini-supercell type and occurred during Germany's tornado high season,
2. the tornado formed after the parent storm entered the hilly terrain of the Neckar valley which also lead to a modified track of the thunderstorm cell,
3. the tornado vortex touched down north (i. e. left) of the in-cloud mesocyclone's ground track,
4. both anticyclonic false hook echo and its anticyclonic small vortex signature were most likely caused by orogenic forcing of the low-level flow in the Neckar valley,
5. contrary to the Nußbach tornado which dissipated within hilly terrain, the Ziegelhausen tornado was generated by small-scale terrain forcing effects, from a thunderstorm which may otherwise not have become tornadic.

The storm's tornadic potential was not detected in advance. No tornado watch or warning was issued.

## Acknowledgments

Dr. E. Baader from Forstamt Heidelberg provided detailed information on the tornado's damage swath. A referee's hint on the dynamics of false hooks stimulated the interpretation of our results and is kindly acknowledged. Please check <http://www.op.dlr.de/~pa4p/TorDACH/> for updates of the data presented in this paper.

## References

Brooks, H. E., C. A. Doswell, J. Cooper, 1994: On the environments of tornadic and nontornadic mesocyclones. *Wea. Forecasting* **9**, 606–618.

Dittmar, R., 1998: *Der Ziegelhäuser Sturm. Untersuchung der Wiederbewaldungsprozesse auf Sturmwurfflächen des Jahres 1996 im Forstbezirk Heidelberg*. Referendararbeit am Staatl. Forstamt Heidelberg, 64 pp.

Dotzek, N., 1999: *Mesoskalige numerische Simulation von Wolken- und Niederschlagsprozessen über strukturiertem Gelände*. Diss., Univ. Karlsruhe, 127 pp.  
[<http://www.op.dlr.de/~pa4p/>]

Dotzek, N., 2000: Tornadoes in Germany. Submitted to *Atmos. Res.*  
[<http://www.op.dlr.de/~pa4p/TorDACH/>]

Dotzek, N., R. Hannesen, K. D. Beheng, R. E. Peterson, 1998: Tornadoes in Germany, Austria, and Switzerland. *Proc. 19th Conf. on Severe Local Storms*, Minneapolis, 93–96.

Dotzek, N., G. Berz, E. Rauch, R. E. Peterson, 2000: Die Bedeutung von Johannes P. Letzmanns “Richtlinien zur Erforschung von Tromben, Tornados, Wasserdosen und Kleintromben” für die heutige Tornadoforschung. *Meteor. Z.* **9**, 137–146.  
[<http://www.op.dlr.de/~pa4p/TorDACH/>]

Finke, U., T. Hauf, 1996: The characteristics of lightning occurrence in southern Germany. *Contr. Atmos. Phys.* **69**, 361–374.

Gysi, H., 1998: Orographic influence on the distribution of accumulated rainfall with different wind directions. *Atmos. Res.* **47–48**, 615–633.

Hagen, M., B. Bartenschlager, U. Finke, 1999: Motion characteristics of thunderstorms in southern Germany. *Meteor. Appl.* **6**, 227–239.

Hannesen, R., 1998: *Analyse konvektiver Niederschlagssysteme mit einem C-Band Doppler-radar in orographisch gegliedertem Gelände*. Diss., Univ. Karlsruhe, 119 pp.

Hannesen, R., N. Dotzek, H. Gysi, K. D. Beheng, 1998: Case study of a tornado in the Upper Rhine valley. *Meteor. Z.*, N. F. **7**, 163–170. [<http://www.op.dlr.de/~pa4p/TorDACH/>]

Höller, H., U. Finke, H. Huntrieser, M. Hagen, C. Feigl, 1999: Lightning-produced NO<sub>x</sub> (LINOX): Experimental design and case study results. *J. Geophys. Res.* **104D**, 13 911–13 922.

Houze, R. A., W. Schmid, R. G. Fovell, H.-H. Schiesser, 1993: Hailstorms in Switzerland: Left movers, right movers, and false hooks. *Mon. Wea. Rev.* **121**, 3345–3370.

Huntrieser, H., H. Schlager, C. Feigl, H. Höller, 1998: Transport and production of NO<sub>x</sub> in electrified thunderstorms: Survey of previous studies and new observations at mid-latitudes. *J. Geophys. Res.* **103D**, 28 247–28 264.

Kennedy, P. C., N. E. Westcott, R. W. Scott, 1993: Single-Doppler radar observations of a mini-supercell tornadic thunderstorm. *Mon. Wea. Rev.* **121**, 1860–1870.

Peterson, R. E., 1992: Johannes Letzmann: A pioneer in the study of tornadoes. *Wea. Forecasting* **7**, 166–184.

Schmid, W., H.-H. Schiesser, B. Bauer-Messmer, 1997: Supercell storms in Switzerland: Case studies and implications for nowcasting severe winds with Doppler radar. *Meteor. Appl.* **4**, 49–67.

Suzuki, O., H. Niino, H. Ohno, H. Nirasawa, 2000: Tornado-producing mini supercells associated with typhoon 9019. *Mon. Wea. Rev.* **128**, 1868–1882.

Terpstra, E., 2000: Supercells in the Netherlands. *Preprints 1st Conf. on European Tornadoes and Severe Storms*, Toulouse, 1 p.

Wegener, A., 1917: *Wind- und Wasserhosen in Europa*. Vieweg, Braunschweig, 301 pp.

## Tables

Table 1: Life–cycle of the tornado’s parent storm. Maximum reflectivities  $Z_{\max}$  and echo tops  $H_{25 \text{ dBZ}}$  are shown for each radar volume scan time as well as a brief characteristic of storm evolution. The position numbers from Fig. 3 are also given. **T** denotes tornado touchdown.

Scan time UTC	$Z_{\max}$ dBZ	$H_{25 \text{ dBZ}}$ km	Fig. 3	Remarks
16:48	45–50	10.0	–	line echo SW–NE
16:58	45–50	9.5	1	broad line SW–NE
17:08	45–50	8.5	2	undular line SW–NE
17:18	45–50	9.0	3	straight line SSW–NNE
17:28	45–50	10.0	4	line echo SSW–NNE
17:38	50–55	12.0	5	bow–line echo
17:48	55–60	12.0	6	2 cores, attenuation
17:58	50–55	12.5	7	1 core, <b>T</b> , attenuation
18:08	55–60	12.5	8	1 core, <b>T</b> , attenuation
18:18	50–55	11.5	9	strongest attenuation
18:28	55–60	11.0	10	strong attenuation
18:38	50–55	11.0	–	cell broadening
18:48	50–55	11.0	–	4 cores
18:58	50–55	10.5	–	2 cores
19:08	45–50	10.5	–	2 cores
19:18	45–50	10.5	–	2 cores

## Figure captions

Figure 1: Geographical map of Karlsruhe radar's 120 km operational range. Rivers are given as solid lines, orography in 200 m steps (white = below 200 m, darkest grey = above 600 m ASL). **H** = Heidelberg, **Z** = Ziegelhausen, **Ka** = Karlsruhe, **N** = Nußbach at the orifice of the Renn valley.

Figure 2: NOAA satellite picture of 23 July 1996, 1200 UTC, with an overlay of synoptic structures (from a weather chart) at that time. A long convergence line roughly 350 km E of the actual frontal zones induces deep convection over Central Europe.

Figure 3: Ground track of parent thunderstorm (bullets) and tornado position (arrow, **T**). The radar scan times are 1 = 1658 UTC to 10 = 1828 UTC in 10 min intervals (cf. Tab. 1). Terrain height contour shading as in Fig. 1. Range rings are drawn every 20 km.

Figure 4: Composite of reflectivity and Doppler velocity data at 1808 UTC (a) and 1828 UTC (b). Greyscale shading gives terrain height as in Fig. 1. The hatched region shows the 20 dBZ area, cross-hatching is applied for  $Z \geq 43$  dBZ. Large open ring arrows denote location of the mesocyclone, the small ring arrow indicates the low-level anticyclonic rotation at the hook echo tip. Tornado position is marked by the thin straight arrow (**T**).

Figure 5: Small-scale sketch map of the probable low-level flow field (bold solid arrows) around Königstuhl mountain, the storm track (open dashed arrow), and tornado damage swath (bold dashed line). Direction to Karlsruhe radar is also indicated.

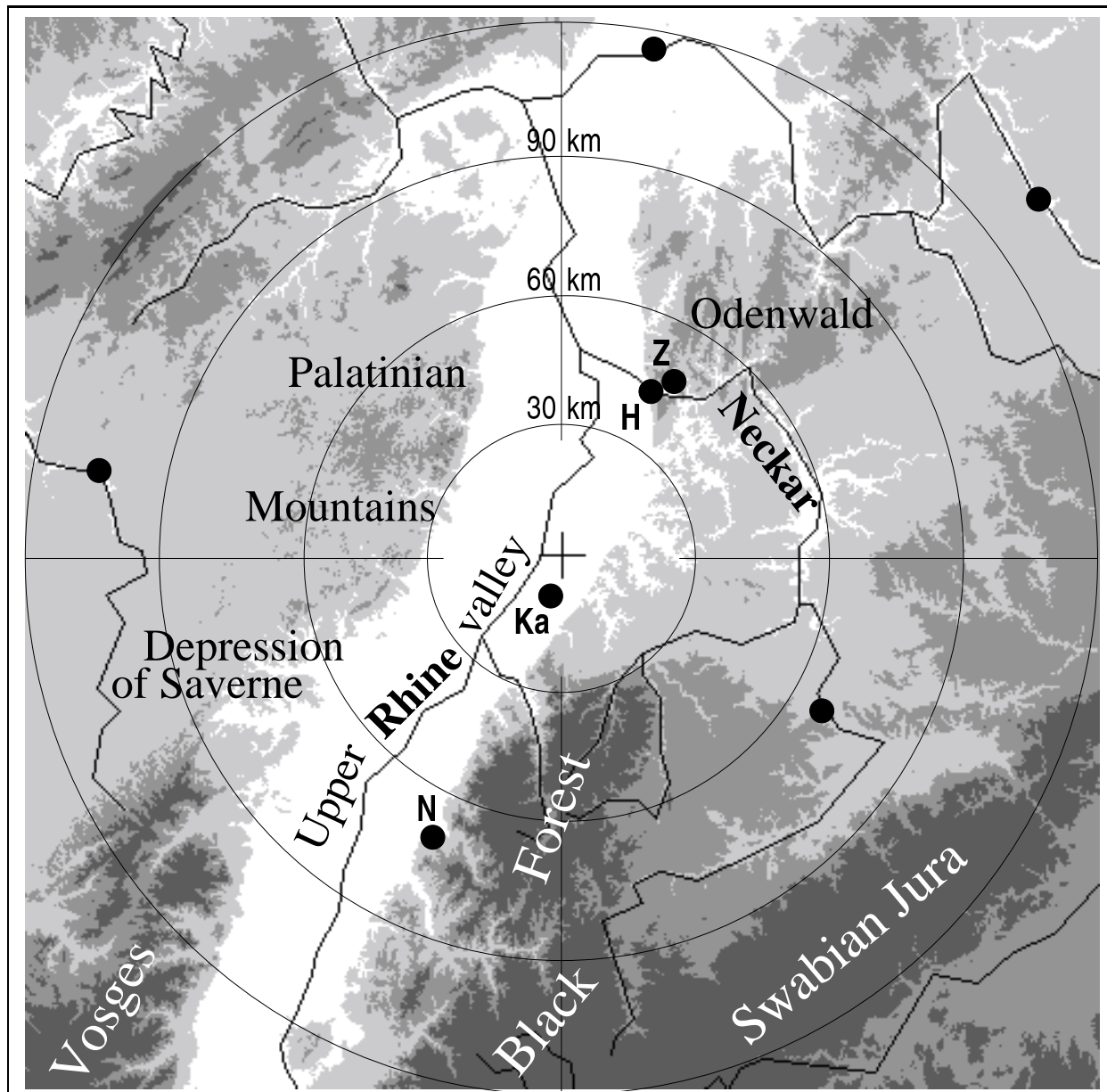


Figure 1

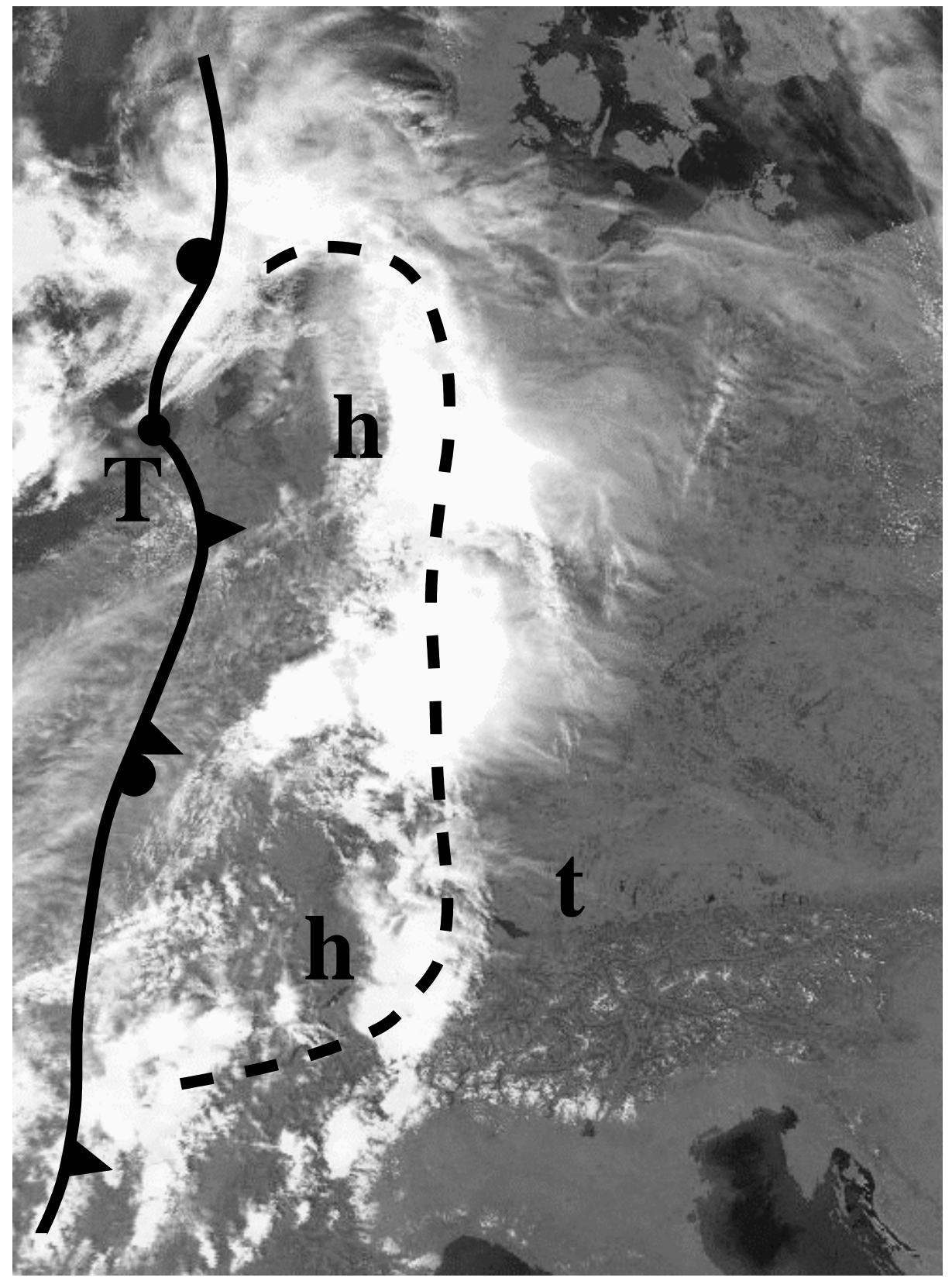


Figure 2

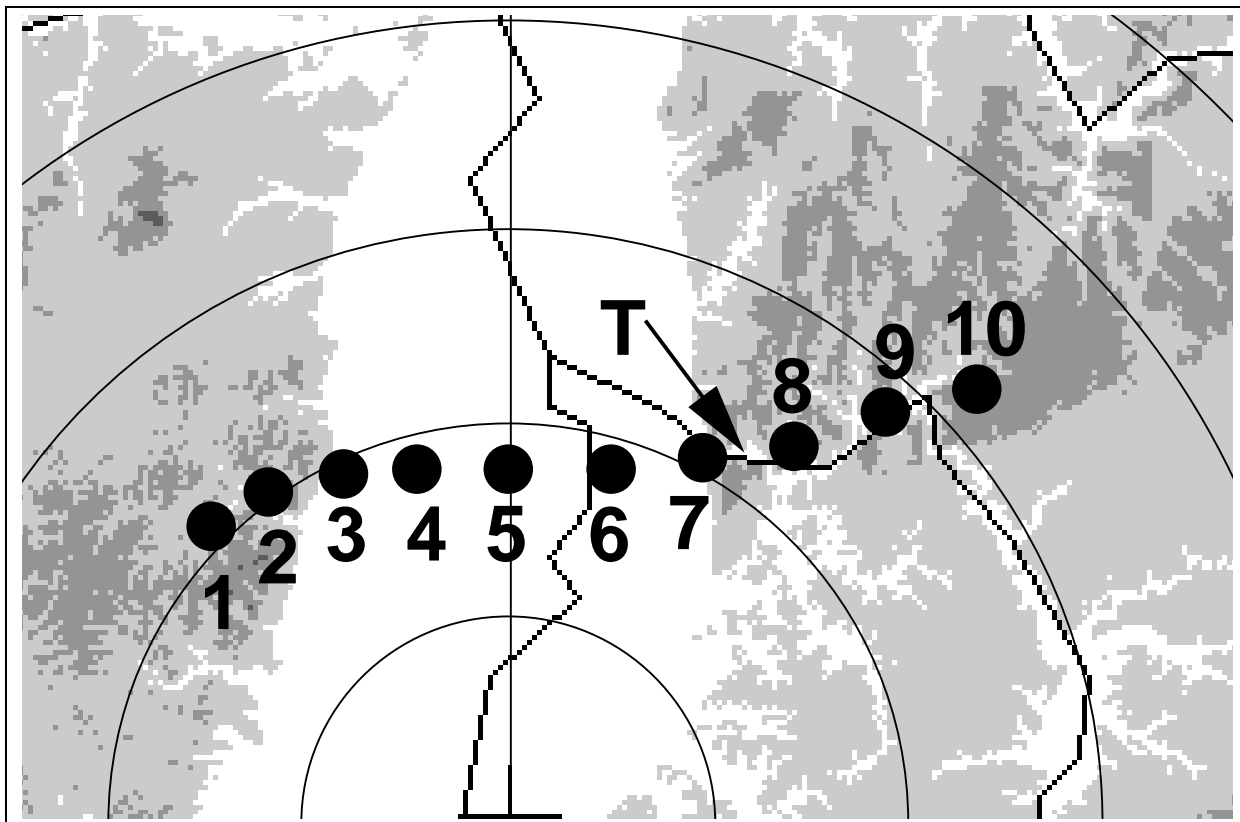


Figure 3

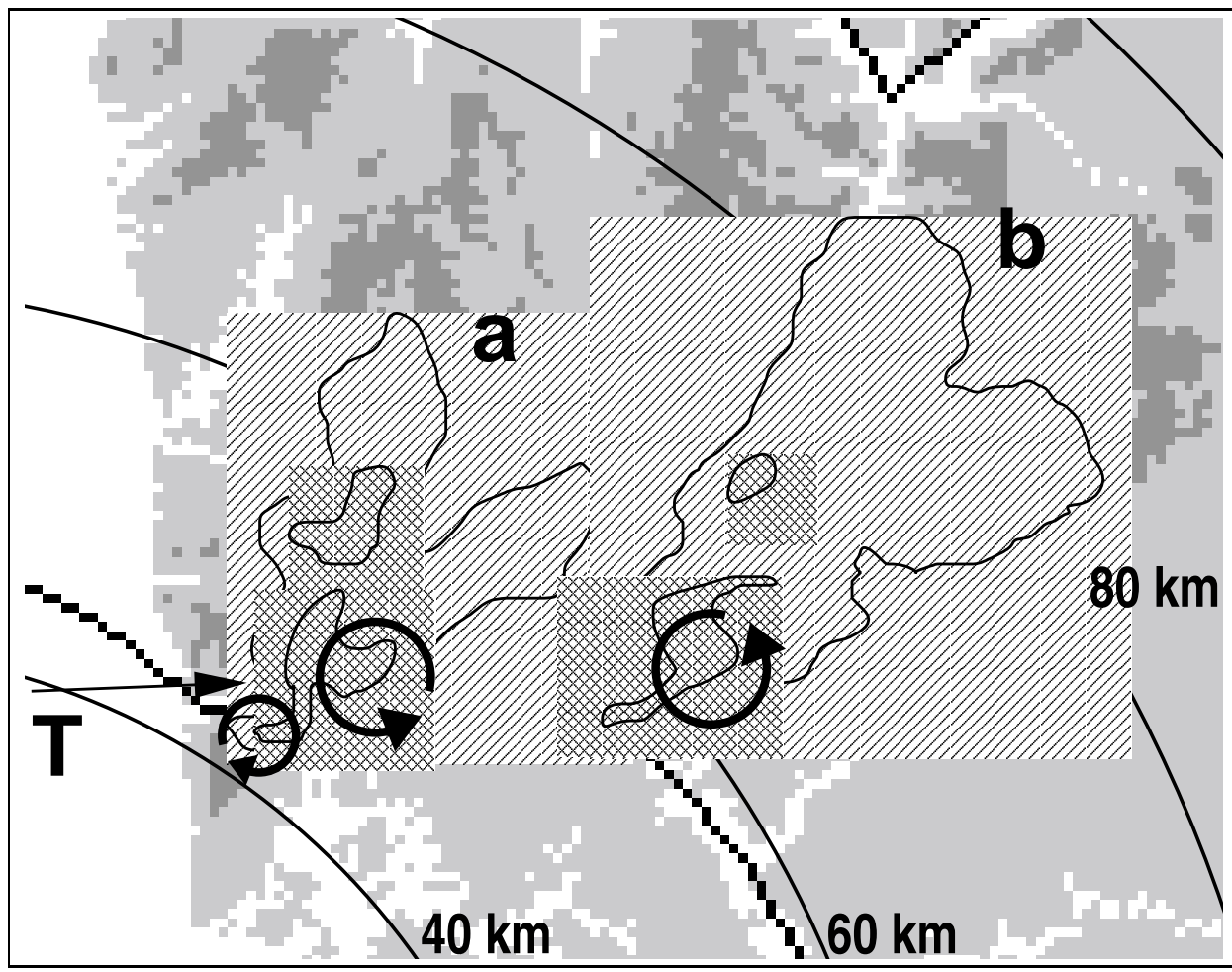


Figure 4

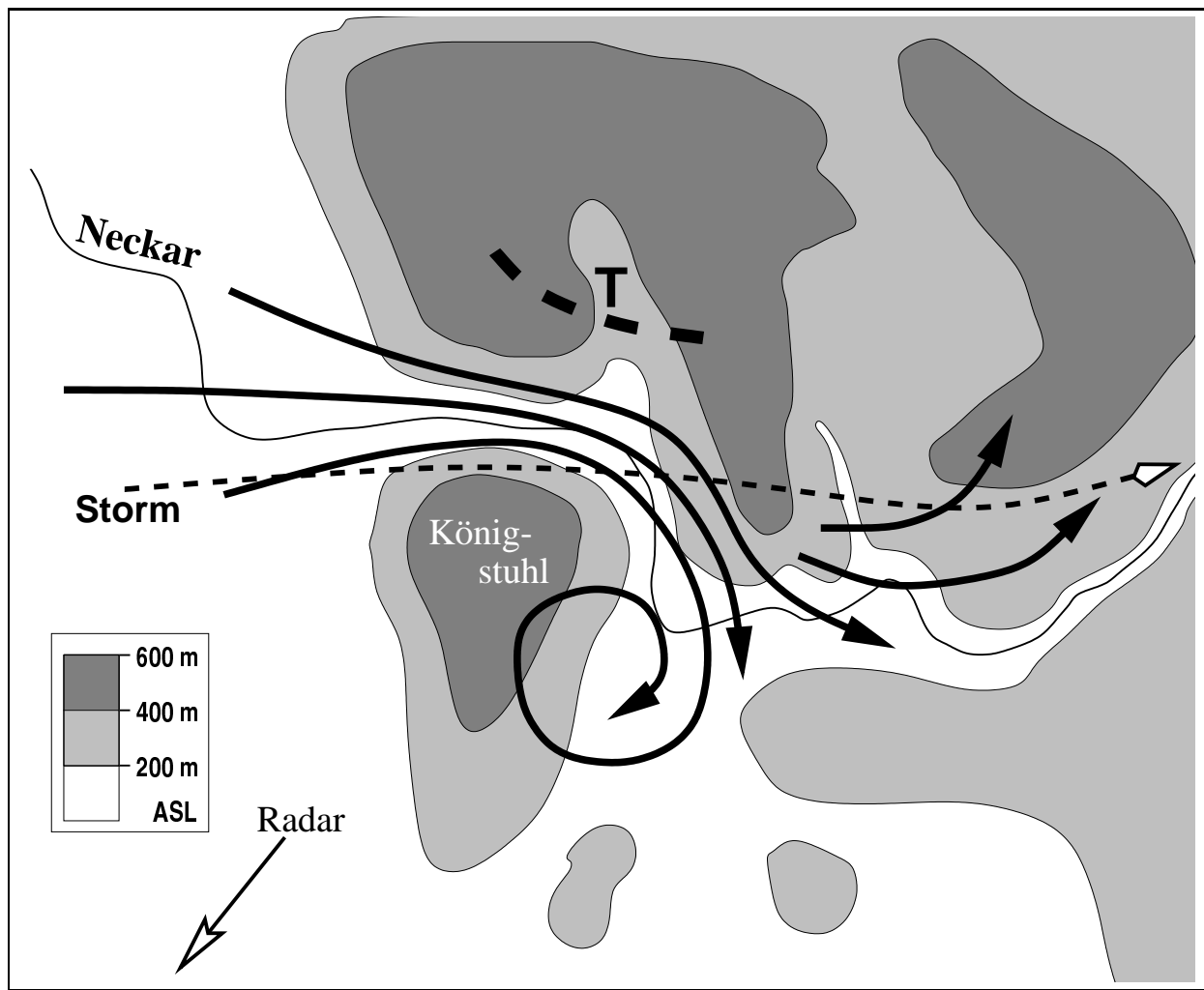


Figure 5